Finite-temperature phase diagram of ultrathin magnetic films without external fields

Santiago A. Pighin,[1,*] Orlando V. Billoni,[2,†] and Sergio A. Cannas[2,‡]

[1]*Centro Atómico Bariloche, Comisión Nacional de Energía Atómica (CNEA, CONICET) Avenida E. Bustillo 9500,
R8402AGP S.C. de Bariloche, Argentina*

[2]*Facultad de Matemática, Astronomía y Física, Universidad Nacional de Córdoba, Instituto de Física Enrique Gaviola (IFEG-CONICET)
Ciudad Universitaria, 5000 Córdoba, Argentina*

We analyze the finite-temperature phase diagram of ultrathin magnetic films by introducing a mean-field theory, valid in the low-anisotropy regime, i.e., close to the spin reorientation transition. The theoretical results are compared with Monte Carlo simulations carried out on a microscopic Heisenberg model. Connections between the finite-temperature behavior and the ground-state properties of the system are established. Several properties of the stripe pattern, such as the presence of canted states, the stripe width variation phenomenon, and the associated magnetization profiles, are also analyzed.

I. INTRODUCTION

Despite the increasing growth of knowledge about magnetic ordering in ultrathin magnetic films during the last decade, from both experimental [1–10] and theoretical [7,11–17] work, there are still many open questions, especially regarding its finite-temperature behavior. One of the main obstacles to advance in these studies is the long-range character of the dipolar interactions, which are fundamental to explain pattern formation in those systems. In particular, numerical simulations, although they have been of great aid [18–25], are strongly limited by finite-size effects. To avoid them, the system size must be large enough to contain a large number of domains. The main problem relates not to the direct influence of dipolar interactions on the boundary conditions, but to the fact that the basic spatial scale for these systems, namely, the typical domain size, scales exponentially with the exchange–to–dipolar coupling ratio δ at very low temperatures [26] and is roughly linear with δ close to the transition to a disordered state [2,7,27]. Typical values of δ in ultrathin magnetic films, like Fe-based films, are about $\delta \sim 100$ [16], thus implying the necessity for very large system sizes to accommodate a reasonable number of domains. To perform simulations with those sizes has represented, up to now, a formidable task, even in the best case (close to the transition). Therefore, knowledge about how the different thermodynamical properties scale with δ would be very helpful for estimattion of whether the numerical results for relatively small values of δ (typically between 3 and 5 to date) can be extrapolated to more realistic values.

For analysis of the magnetic properties of ultrathin films, the out-of-plane anisotropy–to–dipolar coupling η is also important. The system behavior appears to be strongly dependent on experimental features that modify it, such as the film thickness and the sample preparation conditions. A strong dependence is also observed in numerical simulations for $\delta = 3$ [23]. For low

η values, a spin reorientation transition (SRT) from a uniformly magnetized planar phase into a perpendicular striped phase can happen at finite temperature T (in the absence of an external field), in agreement with a previous theoretical prediction [28]. On the other hand, for high values of η there is no planar ferromagnetic (PF) phase and the system undergoes a direct transition from the striped state to a disordered one. From these numerical results a global (η, T) phase diagram was obtained, which is in qualitative agreement with a variety of experimental results [23]. However, for such a small value of δ certain features can be very different from those expected for large values of δ. For instance, at zero temperature the striped equilibrium state for η above certain critical value η_c (where the SRT occurs) is characterized by a stripe width almost independent of η for $\delta < 5$. On the contrary, for values of $\delta \geqslant 5$, a strong variation of the equilibrium stripe width with η emerges when $\eta > \eta_c$ [16]. Another feature that depends strongly on the interplay between exchange and anisotropy is the structure of the magnetization pattern close to the SRT. At zero temperature and close to the SRT, the out-of-plane component of the magnetization presents an almost-sinusoidal shape with a large in-plane component, displaying a canted structure [16]. For small values of δ ($\delta < 5$) such a structure remains for a relatively large interval of values of η above the SRT and changes abruptly to a completely perpendicular striped state with sharp domain walls (Ising-like state). Consistently, numerical evidence of a canted structure with a sinusoidally shaped magnetization profile close to the SRT at finite temperature has recently been reported for $\delta = 4.5$ [24]. However, as δ increases, the range of anisotropy values at which this canted state is present shrinks at zero temperature [16], becoming almost negligible for realistic values of δ. Hence, it is not clear whether or not it is expected to be relevant at finite temperature.

In this work we analyze the finite-temperature phase diagram in the low-anisotropy region (close to the SRT) and several related properties using a coarse-grained based mean-field model for ultrathin magnetic films and Monte Carlo (MC) simulations on a microscopic model. The main objective of the paper is to discuss which of the observed features of the phase diagram for low values of δ are expected

---

*spighin@cab.cnea.gov.ar
†billoni@famaf.unc.edu.ar
‡cannas@famaf.unc.edu.ar

to reflect the large-δ behavior. Several properties of stripe patterns are also analyzed. The plan of the paper is as follows: in Sec. II we introduce the coarse-grained model and calculate the associated mean-field phase diagram. In Sec. III we present MC simulation results for a Heisenberg model and compare them with the previous ones. In Sec. IV we discuss our results.

II. THE MEAN-FIELD MODEL

We consider a general phenomenological Landau-Ginzburg free energy for a two-dimensional ultrathin magnetic film of the form

$$
\begin{aligned}
F[\mathbf{M}] = \frac{1}{2} \int d^2\mathbf{x} &\left\{ (\nabla\mathbf{M}(\mathbf{x}))^2 + r_0\mathbf{M}^2(\mathbf{x}) + \frac{u}{2}\mathbf{M}^4(\mathbf{x}) \right\} \\
&+ \frac{1}{2\delta} \int d^2\mathbf{x} \int d^2\mathbf{x}' \\
&\times \left[\frac{\mathbf{M}(\mathbf{x}) \cdot \mathbf{M}(\mathbf{x}') - 3(\mathbf{n}\cdot\mathbf{M}(\mathbf{x}))(\mathbf{n}\cdot\mathbf{M}(\mathbf{x}'))}{|\mathbf{x}-\mathbf{x}'|^3} \right] \\
&- \frac{\eta}{\delta} \int d^2\mathbf{x}\, M_z^2(\mathbf{x}),
\end{aligned} \tag{1}
$$

where $\mathbf{M} = (M_x, M_y, M_z)$ is the coarse-grained magnetization, δ is the exchange-to-dipolar coupling ratio, η is the anisotropy-to-dipolar coupling ratio, and $\mathbf{n}$ is a unit vector pointing in the $\mathbf{x}-\mathbf{x}'$ direction. A cutoff at some microscopic scale Λ is implied in the second integral. We assume $\Lambda = 1$. The temperature dependency comes through $r_0 = r_0(T)$.

In order to minimize Eq. (1), we propose a variational stripe-like solution, i.e., a modulated solution along the y direction, where only Bloch walls between domains are allowed [26], namely, $\mathbf{M}(\mathbf{x}) = \mathbf{M}(x)$ and $M_x(x) = 0$. We also assume that the modulus of the magnetization is uniform, i.e.,

$$
M_y^2(x) + M_z^2(x) = M^2 \; \forall \, x.
$$

This approximation is expected to break down for large enough values of η, where the statistical weight of spin configurations with large in-plane components tends to 0, but nonuniform out-of-plane configurations are still expected to minimize the free energy [17]. In fact, in the $\eta \to \infty$ limit the whole effective free energy, (1), ceases to be valid, being replaced by a functional of a scalar order parameter (local out-of-plane magnetization), without the anisotropy term [17].

Under the present assumptions, the following form of the dipolar term can be assumed [27]:

$$
\frac{L}{\delta} \int dx \int dx' \frac{M_z(x)M_z(x')}{|\mathbf{x}-\mathbf{x}'|^2},
$$

where we have neglected the self-energy term arising from the dipolar energy, since it just implies a constant shift in the anisotropy coefficient η. Then the variational free energy per unit area reduces to

$$
\begin{aligned}
f[\mathbf{M}] = \frac{1}{2L} \int dx &\left\{ \left(\frac{\partial M_y}{\partial x}\right)^2 + \left(\frac{\partial M_z}{\partial x}\right)^2 + r_0 M^2 + \frac{u}{2}M^4 \right\} \\
&+ \frac{1}{\delta L} \int dx \int dx' \frac{M_z(x)M_z(x')}{(x-x')^2} - \frac{\kappa}{L\delta} \int dx\, M_z^2(x),
\end{aligned} \tag{2}
$$

where $\kappa = \eta - \alpha$ with $\alpha = 3.485\ldots$ [16]. We can write $M_z(x) = M\,\phi(x)$, where $|\phi(x)| \leqslant 1$. Then

$$
f = \frac{1}{2}(r_0(T) + 2\,e/\delta)M^2 + \frac{u}{4}M^4, \tag{3}
$$

where

$$
\begin{aligned}
e[\phi(x)] = \frac{\delta}{2L} \int dx &\left\{ \left(\frac{\partial\sqrt{1-\phi^2}}{\partial x}\right)^2 + \left(\frac{\partial\phi}{\partial x}\right)^2 \right\} \\
&+ \frac{1}{L} \int dx \int dx' \frac{\phi(x)\phi(x')}{(x-x')^2} - \frac{\kappa}{L} \int dx\,\phi^2(x),
\end{aligned} \tag{4}
$$

i.e., $e[\phi(x)]$ is the microscopic energy per spin of the associated microscopic model (Heisenberg model with out-of-plane anisotropy, exchange, and dipolar interactions) for a spin density profile $(S^x(x), S^y(x), S^z(x)) = (0, \sqrt{1-\phi(x)}, \phi(x))$. Its minimal energy configuration as a function of the microscopic parameters (δ, η) can be described by variational expressions characterized by different sets of variational parameters $p_1, p_2, \ldots$, which are described later. Minimization of the free energy, Eq. (3), leads to

$$
\frac{\partial f}{\partial M} = M(r_0 + 2\,e(p_1, p_2, \ldots)/\delta + u\,M^2) = 0, \tag{5}
$$

$$
\frac{\partial f}{\partial p_i} = \frac{M^2}{\delta}\frac{\partial e}{\partial p_i} = 0. \tag{6}
$$

We also have

$$
\frac{\partial^2 f}{\partial M^2} = r_0 + 2e/\delta + 3uM^2, \tag{7}
$$

$$
\frac{\partial^2 f}{\partial M\,\partial p_i} = \frac{2M}{\delta}\frac{\partial e}{\partial p_i}, \tag{8}
$$

and

$$
\frac{\partial^2 f}{\partial p_i\,\partial p_j} = \frac{1}{\delta}M^2\frac{\partial^2 e}{\partial p_i\,\partial p_j}. \tag{9}
$$

$M = 0$ is always a solution of the extremal equations (5) and (6) and the corresponding free energy $f = 0$ is independent of the parameter values of $(p_1, p_2, \ldots)$. Hence, all the second derivatives are 0, except

$$
\left.\frac{\partial^2 f}{\partial M^2}\right|_{M=0} = r_0 + 2e/\delta, \tag{10}
$$

which controls the stability of the $M = 0$ solution.

An ordered solution (local minimum of f) with $M \neq 0$ exists whenever $r_0 + 2\,e/\delta < 0$. From Eqs. (5) and (6) we have that

$$
M^2 = -(r_0 + 2e/\delta)/u \tag{11}
$$

and

$$
\frac{\partial e}{\partial p_j} = 0. \tag{12}
$$

Hence, from Eqs. (7) and (11) it follows that

$$
\frac{\partial^2 f}{\partial M^2} = 2uM^2,
$$

and from Eqs. (8) and (12),

$$
\frac{\partial^2 f}{\partial M\,\partial p_i} = 0.
$$

Then the Hessian matrix of f has a positive eigenvalue $2uM^2$ and a diagonal block that equals $M^2 H_e/\delta$, where H_e is the Hessian matrix of e. Therefore, a local minimum of f has to be a local minimum of e. The free energy of an ordered phase is

$$f = -\frac{1}{4u}(r_0(T) + 2e_{\min}/\delta)^2. \tag{13}$$

The extremal properties of e are well known [16,27]. For low values of the anisotropy η the minimum of e corresponds to a PF configuration $\phi(x) = 0$. Above a certain critical value $\eta_c(\delta) = \alpha + \pi^2/3 - \pi^2/2\delta$ [16,27], e is minimized by a striped profile with periodicity $2h$ (h is the stripe width). Close to η_c the domain structure corresponds to a canted sinusoidal wall profile (SWP), where $|\phi(x)| = \cos\theta$ is constant inside the striped domains ($0 \leqslant \theta \leqslant \pi/2$ is the canting angle) and presents a sinusoidal structured wall of width w [27]. The energy of the SWP is given by

$$
\begin{aligned}
e_{\text{SWP}}(s,k,\Delta) = {} & \frac{\delta k^2}{2\Delta}(1 - \sqrt{1-s^2}) \\
& + s^2\left((\pi^2/3 - \eta)(1 - \Delta/2) - \frac{\pi k}{2}G(\Delta)\right),
\end{aligned}
\tag{14}
$$

where $s = \cos\theta$, $k \equiv \pi/h$, a $\Delta \equiv w/h$, and [27]

$$G(\Delta) = \frac{16}{\pi^2}\sum_{m=1,3,\dots}\frac{1}{m(1-m^2\Delta^2)^2}\cos^2\left(\frac{\pi m\Delta}{2}\right). \tag{15}$$

Different approximations of a high accuracy for $G(\Delta)$ are available [2,27], so the values of (s,k,Δ) that minimize Eq. (14) can be found numerically for arbitrary values of (δ,η). As the value of η is raised above η_c the canting angle decreases rapidly from $\theta = \pi/2$ at $\eta = \eta_c$ to $\theta \approx 0$ and the striped pattern that minimizes e changes to a hyperbolic wall (HPW) magnetization profile whose energy is given by [16]

$$e_{\text{HPW}}(k,\Delta) = \gamma(1 - \Delta/2) + \frac{4\delta}{\pi^2}\frac{k^2}{\Delta} - \frac{4k}{\pi}\ln\left(\frac{6\pi}{5\Delta}\right), \tag{16}$$

where $\gamma = A - \eta$, with $A = 4.5327\dots$. Equation (16) can be easily minimized [16].

If $r_0 < 0$ and $\eta < \eta_c$ ($e_{\min} = 0$), the global minimum of f corresponds to $M^2 = -r_0/u$ and $s = 0$, that is, to a PF state with free energy $f = -r_0^2/4u$. When $r_0 = 0$ and $\eta < \eta_c$ the system undergoes a second-order phase transition between the paramagnetic state and the PF one, independently of η. We assume hereafter that $r_0 = a(T - T_F)$, where T_F is the paramagnetic-to-PF transition temperature.

When $T < T_F$ and $\eta \geqslant \eta_c$ the SWP configuration with free energy given by Eq. (13) is the stable solution for values of η close to η_c. Since the striped order emerges continuously, the SRT at $\eta = \eta_c$, according to the present approximation, is a second-order one. As η is further increased there is an energy crossing at a certain value of η and the stable configuration changes into an HWP. Hence, for $\eta_c \leqslant \eta \leqslant \eta^*$
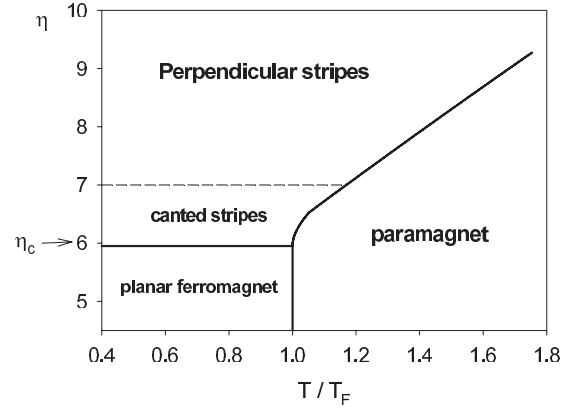
FIG. 1. Mean-field phase diagram for $\delta = 6$ and $a/T_F = 1$. Solid lines correspond to second-order phase transitions. The dashed line marks the crossover between canted-stripe and perpendicular-stripe configurations; it is estimated arbitrarily as the region above which the maximum in-plane component of the magnetization is less than 5% of the saturation magnetization M ($s < 0.05$).

the stable configuration is a canted striped one, while for $\eta > \eta^*$ the stripes are fully saturated in the out-of-plane direction inside the domains (we call this state an "Ising striped configuration").

If $T > T_F$ ($r_0 > 0$) and $\eta > \eta_c$, the global minimum corresponds to the modulated phase when $r_0 + 2e_{\min}/\delta < 0$, i.e., $T > T_F - 2e_{\min}/a\delta$. Therefore, there is a transition line at $T_c(\eta) = T_F - 2e_{\min}(\eta)/a\delta$. The order parameter changes continuously at T_c ($M^2 = -(r_0 + 2e_{\min}) = 0$), but s changes discontinuously. In Fig. 1 we illustrate the typical topology of the phase diagram for the particular case $\delta = 6$. All the solid lines in Fig. 1 correspond to second-order phase transitions. We also show the crossover line between the region where the magnetization profile shows a significant canting angle (canted stripes) and the region where the local magnetization is almost perpendicular to the plane (perpendicular stripes).

Although the paramagnetic solution is not a global minimum of f when $\eta > \eta_c$ and $T > T_F$, it could still be a local minimum provided that $r_0 + G < 0$ for some values of s and k_0. From Eq. (10), this condition ensures the local stability against variations of M. However, since all the rest of the second derivatives cancel, complete stability of the paramagnetic solution is beyond the linear analysis. We verified numerically that indeed the paramagnetic phase remains locally stable (metastable) below $T = T_F$ at a fixed $\eta > \eta_c$. Such metastability is a result of the high degeneracy of the paramagnetic solution under the present approximation, so it appears to be a spurious result. However, it can be indicative of a change in the order of the transition if the approximation is improved. Indeed, there are several lines of evidence indicating the first-order nature of the stripe-disordered phase transition [11,19,23].

III. MONTE CARLO SIMULATIONS

In order to compare the mean-field results with the behavior of a specific microscopic model, we performed MC simulations using a Heisenberg model with exchange and dipolar interactions, as well as uniaxial out-of-plane

anisotropy. The model, which describes an ultrathin magnetic film (see Ref. [16] and references therein) can be characterized by the dimensionless Hamiltonian,

$$\mathcal{H} = -\delta \sum_{\langle i,j \rangle} \vec{S}_i \cdot \vec{S}_j + \sum_{(i,j)} \left[\frac{\vec{S}_i \cdot \vec{S}_j}{r_{ij}^3} - 3 \frac{(\vec{S}_i \cdot \vec{r}_{ij})(\vec{S}_j \cdot \vec{r}_{ij})}{r_{ij}^5} \right] - \eta \sum_i (S_i^z)^2, \tag{17}$$

where the exchange and anisotropy constants are normalized relative to the dipolar coupling constant, $\langle i,j \rangle$ stands for a sum over nearest-neighbor pairs of sites in a square lattice with $N = L_x \times L_y$ sites (the lattice parameter is taken equal to 1), (i,j) stands for a sum over *all distinct* pairs and $r_{ij} \equiv |\vec{r}_i - \vec{r}_j|$ is the distance between spin i and spin j. Each spin is defined by a unit vector with components S^x, S^y, and S^z. All the simulations were done using the Metropolis algorithm, and periodic boundary conditions were imposed on the lattice by means of the Ewald sum technique. We focus our simulations on the case $\delta = 6$, where the system presents a canted equilibrium state at zero temperature for a wide range of anisotropy values [16].

The phase diagram was obtained by measuring the out-of-plane magnetization,

$$M_z \equiv \frac{1}{N} \sum_{\vec{r}} \langle S^z(\vec{r}) \rangle \tag{18}$$

(the in-plane components are defined in a similar way); the in-plane magnetization,

$$M_{||} \equiv \sqrt{(M_x)^2 + (M_y)^2}; \tag{19}$$

and an orientational order parameter [23],

$$O_{hv} \equiv \left\langle \left| \frac{n_h - n_v}{n_h + n_v} \right| \right\rangle, \tag{20}$$

where $\langle \cdots \rangle$ stands for a thermal average, n_h (n_v) is the number of horizontal (vertical) pairs of nearest-neighbor spins with an antialigned perpendicular component, i.e.,

$$n_h = \frac{1}{2} \sum_{\vec{r}} \{1 - \text{sig}[S^z(r_x, r_y), S^z(r_x + 1, r_y)]\}, \tag{21}$$

n_v has a similar definition, and $\text{sig}(x,y)$ is the sign of the product of x and y. To obtain the stripe width of the modulated states we considered the structure factor $|\hat{S}(\vec{k})|^2$, where

$$\hat{S}(\vec{k}) = \frac{1}{\sqrt{N}} \sum_{\vec{r}} S^z(\vec{r}) e^{-i\vec{k} \cdot \vec{r}}. \tag{22}$$

The stripe width was calculated using the expression

$$h = \pi / k_{\max}, \tag{23}$$

where $k_{\max}$ is the modulus of the wave vector that maximizes $|\hat{S}(\vec{k})|^2$.

In order to find the equilibrium phase diagram, we carried out the simulations with two protocols for the independent parameter (temperature, anisotropy, or external field). In the

first protocol, we varied the independent parameter linearly with the simulation time, increasing or decreasing it at a given rate r, keeping the rest of the parameters fixed. For instance, if we choose the temperature, then $T(t) = T(0) + rt$, where t is the simulation time measured in units of Monte Carlo steps (MCSs). Each MCS corresponds to N single-spin updates of the Metropolis algorithm. The initial spin configuration at $T(0)$ was previously obtained by performing t_e MCSs to equilibrate. The order parameters were calculated along the simulation and averaged over many realizations to improve statistics. We call this protocol "linear variation of parameters." The second one was a ladder protocol. For instance, in the case where T is the independent parameter, the system is initialized at the paramagnetic state at a high temperature, and then the temperature is reduced at discrete steps. The initial configuration for each temperature is the last one of the previous step. At each step we discarded the first t_e MCS in order to equilibrate, then we calculated the averages over the next t_m MCS.

First, we calculated $M_{||}$ and O_{hv} as a function of the anisotropy for two fixed temperatures. We applied the linear-variation-of-parameters protocol to increase η from a small value $\eta < \eta_c$, starting from an equilibrated in-plane ferromagnetic configuration. In these simulations we used $L_x = L_y = L$, with $L = 80$ and 120. The parameter variation rate r ranged from $r = 10^{-5}$ to $r = 10^{-7}$, depending on the temperature and the system size. The typical behavior of the order parameters at low temperatures ($T = 0.1$ and $T = 1.0$) is illustrated in Fig. 2. Three behaviors can be identified: the PF state at low anisotropies, characterized by $M_{||} \neq 0$ and $O_{hv} = 0$; a canted-stripe state at intermediate values of η, with both $M_{||} \neq 0$ and $O_{hv} \neq 0$; and a perpendicular-stripe state at
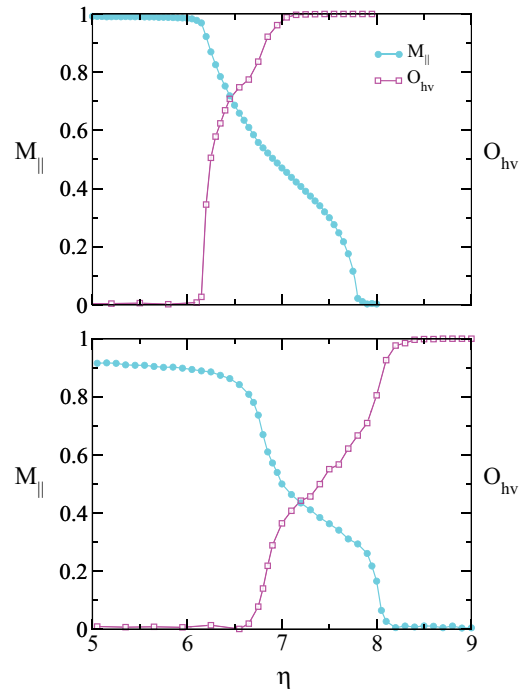
FIG. 2. (Color online) In-plane magnetization and orientational order parameter as a function of anisotropy for $\delta = 6$. $T = 0.1$ (upper panel) and $T = 1.0$ (lower panel).
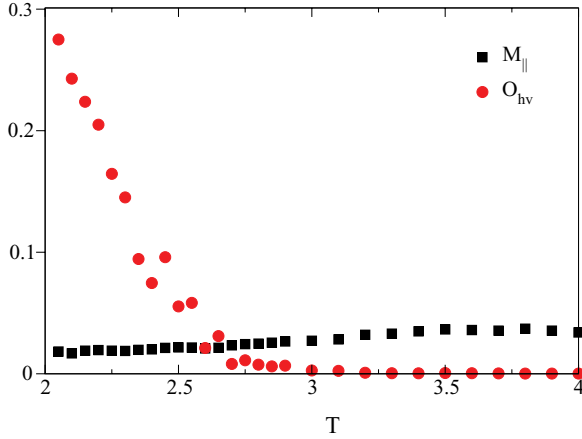
FIG. 3. (Color online) Orientational order parameter [(red) circles] and in-plane magnetization [(black) squares] as a function of temperature for $\delta = 6$ and $\eta = 8.7$.

large enough values of η, characterized by $M_\parallel = 0$ and $O_{hv} \neq 0$. At each temperature the transition points are identified with the values at which the corresponding order parameter becomes 0.

At large anisotropy values ($\eta > 8.4$), the in-plane ferromagnetic phase is absent for any value of the temperature. The system undergoes a direct transition from an almost-perpendicular-stripe state to a paramagnetic state as the temperature is increased. This can be seen in Fig. 3, where the order parameters were computed using a ladder protocol cooling from $T = 4.0$, with $L = 120$, $t_e = 10^5$, and $t_m = 10^5$.

By means of the methods described above, we obtained the phase diagram shown in Fig. 4. Although the global topology of this diagram is in agreement with that obtained by the mean-field theory (see Fig. 1), some noticeable differences exist, which appear to be an artifact of the mean-field approach. Some of them are discussed in Sec. IV. The presence of a canted-stripe region is in agreement with previous MC calculations carried out by Whitehead *et al.* in Ref. [24] for $\delta = 4.5$ and with the zero-temperature behavior of the model [16]. In particular, our results show that the canted region is larger than that corresponding to $\delta = 4.5$.
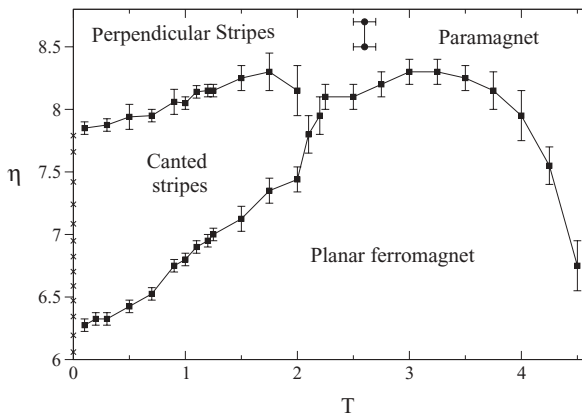
FIG. 4. Monte Carlo phase diagram for $\delta = 6$.
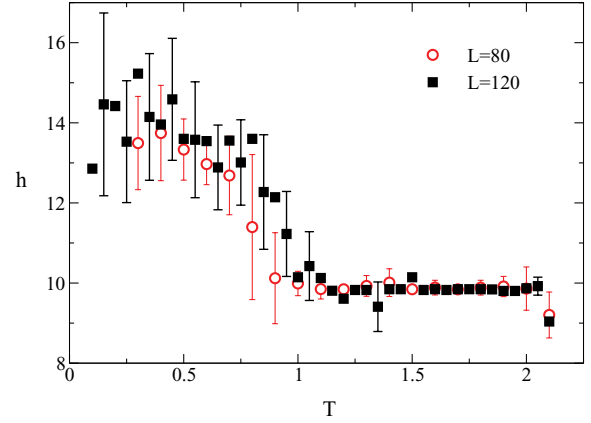
FIG. 5. (Color online) Stripe width as a function of temperature for $\delta = 6$ and $\eta = 7.5$. The simulation parameters were $L = 80$, $r = -10^{-6}$, $t_e = 10^5$, and $t_H = 10^5$ (circles) and $L = 120$, $r- = 10^{-7}$, $t_e = 10^6$, and $t_H = 10^6$ (squares). Error bars are the standard deviations taking into account many realizations; some of them are omitted for clarity.

We explored the canted region looking at the variation of the stripe width h. This is a difficult task because the stripe width variation is mediated by the formation of topological defects (usually stripe dislocations) which need long simulation times to nucleate and move. An acceleration of this process was obtained when we added an in-plane external-field term to Eq. (17) of the form $-\xi \sum_i (S_i^x)$ and applied an LPV protocol with ξ as the free parameter. The value of ξ varies from $\xi(0) = H_x$, where H_x is an external magnetic field strong enough to saturate the magnetization in the x direction, to 0 (zero-field condition). After several tests, we found that $H_x = 0.5$ was optimal for all the regions in the phase diagram studied in this work. Then t_H extra MCSs were performed before calculating h. The stripe width shown as a function of temperature for $\eta = 7.5$ in Fig. 5 is the result of an average performed over several realizations of the LPV protocol and the error bars correspond to the dispersion of h.

The stripe width at the SRT is $h = 10$ and remains constant down to $T = 0.75$, where it displays a steep increase. The widest stripes are observed at low temperatures, reaching a maximum value of $h \sim 14$, close to the zero-temperature value, $h = 17$, calculated previously [16]. The h values obtained for both system sizes are almost undistinguishable, showing that finite-size effects are negligible.

We next analyzed the stripe width variation with the anisotropy, which is closely related to the variation with the film thickness d. Indeed, previous numerical simulations suggest that the effective out-of-plane anisotropy varies inversely with the film thickness $\eta \sim 1/d$ [23]. A common experimental technique to analyze the effects of the film thickness on the magnetic patterns is to take images on wedge-like ultrathin films (e.g., Refs. [2,29]). We modeled these systems assuming the relation $\eta = 1/d(x)$, where $d(x)$ is the local film width, which depends on the x position. The simulations were performed over rectangular lattices of size $L_x = 360$ and $L_y = 180$ using the external field protocol used in the study of the stripe width variation and periodic boundary
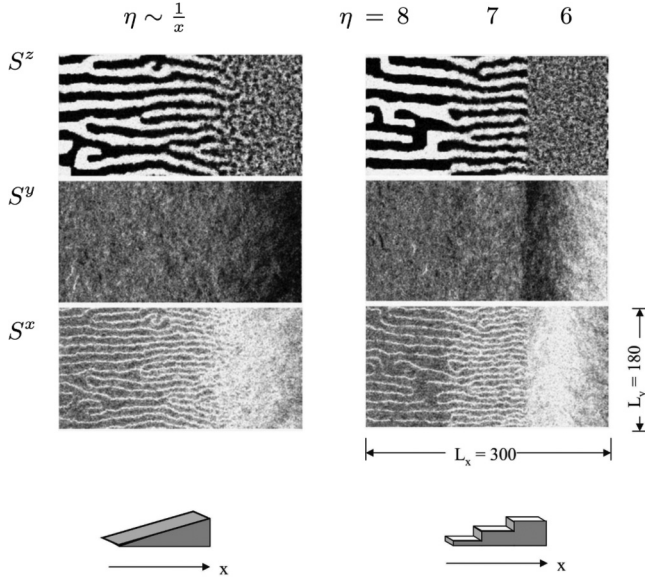
FIG. 6. Snapshots of the spin components for two wedges in equilibrium for $\delta = 6$ at $T = 1$. The film width functional dependence varies as a linear function of x (left) or as equal-spaced steps of values $\eta = 8, 7, 6$ (right), as schematized at the bottom of the columns. Simulation parameters are $r = 10^{-5}$ and $t_e = 10^5$.

FIG. 7. (Color online) Stripe width as a function of η corresponding to the wedge-like film in the left panel in Fig. 6 ($\delta = 6$). The dashed line corresponds to a parabolic fitting.

conditions in the y direction. The results are shown in Fig. 6 in two columns, each column being related to different $d(x)$ assumptions. The left one corresponds to a continuous linear variation of $d(x) = a + bx$, where a and b were chosen such that η varies from $\eta = 6$ at $x = 1$ to $\eta = 8$ at $x = 300$. The right column corresponds to a ladder structure, where $d(x)$ varies at equal-spaced steps corresponding to the values $\eta = 8$, 7, and 6 from left to right. The figure presents typical snapshots of equilibrated magnetic patterns at a fixed temperature. Each pixel represents a spin component in gray scale, ranging from white when the value is 1 to black when it is -1. From the S^z component behavior it turns out that the stripe width decreases as x increases until the SRT. Once the SRT is reached, the spins are ferromagnetically ordered in the same direction as the in-plane component of the magnetization in the walls. Moreover, the S^x components in the walls are along the stripe direction, showing the they are Bloch's walls as expected [26]. Stripe width reduction occurs by the insertion of new stripes from the low-anisotropy (higher thickness) region, in agreement with experimental results on Fe on Cu [1] and Fe/Ni on Cu [2] films. These results give further support to the assumption $\eta \sim 1/d$ and suggest that the observed stripe width variation with film thickness is due to the induced anisotropy gradient. In fact, the $\eta \sim 1/d$ dependency is probably related to the contribution to the effective anisotropy coming from the short-range part of the dipolar energy, which can be assumed tp be proportional to the film thickness [30] (at least in the ultrathin limit). The stripe width variation with η in the wedge-like film in Fig. 6 is shown in Fig. 7. We also performed a series of simulations on lattices with $L_x = L_y$ and uniform anisotropy, for different values of η. The equilibrium average stripe width agreed with that observed in the wedges.
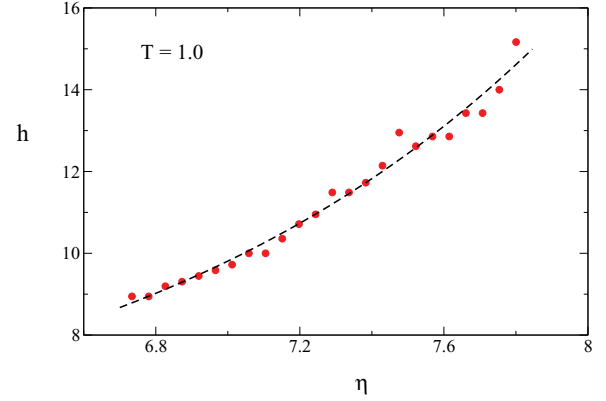
We verified that the increase in the stripe width as η increases follows a series of steps in a similar way to that observed at zero temperature [16]. In other words, the canted region in the phase diagram in Fig. 4 is composed of a series of transition lines (not shown, for clarity) that follow a similar direction as the SRT line and converge to the zero-temperature transition points between different stripe width ground states [16]. Every time the anisotropy crosses one of these lines the stripe width increases by 1 unit (dynamically mediated by defects). In this way, the stripe width variation with temperature (horizontal crossing of those lines in Fig. 4) is related to the ground-state structure of the system. In this context, the absence of stripe width variation with temperature for $\eta > 8.5$ is related to the fact that for $\delta = 6$ the ground-state stripe width has already saturated [16].

Finally, we analyzed the magnetization profile variation of the stripe pattern as a function of anisotropy, which is shown in Fig. 8. These results were obtained by averaging over 25 adjacent profiles $S^z(x, y_0)$ in a system with uniform anisotropy in equilibrium at $T = 0.5$. Topological defects like dislocations were avoided in the calculation. We thermalized the system using the external-field protocol with parameters $L_x = L_y = 144, r = 10^{-5}, t_e = 10^5$, and $t_m = 10^4$. At $\eta = 6.45$ the system
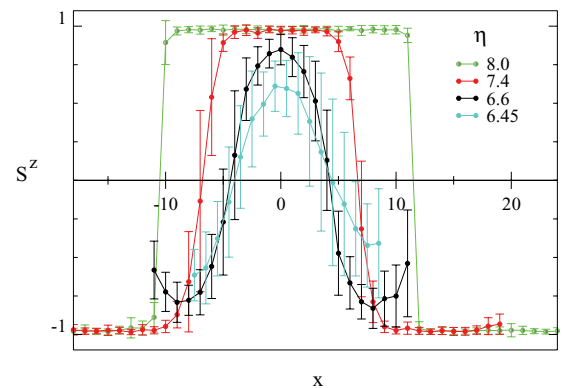
FIG. 8. (Color online) Mean stripe magnetization profiles in the perpendicular direction for $\delta = 6$ at $T = 0.5$. Each curve is the average of consecutive profiles along a stripe, and error bars correspond to standard deviations.

is in the canted state, and the walls are wide with sinusoidal-like shape. The perpendicular components of the spins at the center of the stripes is lower than 1, meaning that all the spins have an in-plane component aligned with the stripes, thus contributing to the in-plane magnetization as pointed out in Fig. 2. As the anisotropy increases, the spins at the center of the stripes become perpendicular to the plane and the walls narrow but are still extended. The same behavior of the magnetization profile is observed at zero temperature [16]. Finally, at high enough anisotropy values ($\eta \geqslant 8.0$), the stripes widen and the wall widths w become close to 1.

It is noteworthy that the fluctuations of the spin directions at low and intermediate anisotropy values are stronger within the walls, as can be observed from the error bars. This suggests that these spins are less restricted from moving and therefore facilitate defect mobility. This explains the higher efficiency of the previously used in-plane field protocol to obtain thermal equilibration, through the interaction between the external field and the large in-plane components inside the walls.

Interestingly, the change in the magnetization stripe profile as the anisotropy increases closely resembles that observed as the temperature decreases, both experimentally [7] and in mean-field theories [7,17].

IV. DISCUSSION

Our mean-field results suggest that the global topology of the phase diagram observed numerically for low values of δ (both from previous [23,24] and from the present simulations) is robust, at least under the validity conditions of the present approximation, namely, in the low-anisotropy region close to the SRT. For large enough values of the anisotropy the approximation breaks down, as evidenced by the unphysical monotonous increase in the transition temperature between the stripe and the paramagnetic phases in the large-η region. This breakdown is on the basis of the present MF approximation, namely, in the effective free energy, Eq. (1). Such a free energy can be obtained variationally from a partition function $\mathcal{Z} = \mathrm{Tr}e^{-\beta H[\mathbf{M}]}$, where the coarse-grained Hamiltonian $H[\mathbf{M}]$ has the same structure as Eq. (1) [31]. The effective free energy $F[\mathbf{M}]$ is then the zero-order term in an expansion of $H[\mathbf{M}]$ around its minimum when fluctuations are neglected. If the $\eta \to \infty$ limit is taken *a priori* of such an expansion, all the configurations with nonzero in-plane magnetization components get zero statistical weight, and a different Landau-Ginzburg free energy (which depends only on the scalar field M^z) is obtained [17]. Therefore, the correct stripe-paramagnet critical temperature must converge to the (η-independent) value predicted by the last free energy when $\eta \gg 1$. In other words, even within the mean-field theory the correct behavior cannot be obtained as the $\eta \to \infty$ limit in the present approach.

While the previous difference (vertical line vs finite slope) between the MC and the MF phase diagrams is specific to the present approach, some others appear to be associated with general features of the mean-field theory. For instance, the transition line between the planar ferromagnet and the canted-stripe phases computed within the MF approximation is horizontal, while it shows a finite slope when extracted from MC simulations. This seems to be a direct effect of

neglecting thermal fluctuations, since theoretical works show that those fluctuations renormalize the dipolar and anisotropy coupling parameters in such a way that the anisotropy $K(T)$ diminishes faster than the dipolar coupling constant $g(T)$ (in our notation, $\eta = K/g$) [28,32]. Those works predict a linear dependence of the reorientation transition temperature with the anisotropy with a positive slope, which is roughly in agreement with the transition lines obtained from MC simulations. Finally, the transition line between the planar ferromagnet and the paramagnetic phases is a vertical straight line in the MF diagram while it shows some slope in the MC diagram. This is because of the simplifying assumption that the (coarse-grained) phenomenological transition temperature T_F is independent of η. While the tendency of the transition line in the MC diagram suggests that this assumption may appropriately describe the very-low-η limit, it clearly fails for large enough values of η. An increase in the perpendicular anisotropy should destabilize the PF phase, thus decreasing the critical temperature.

One fact that emerges, from both our mean-field and our MC results, is the strong influence of the ground-state properties on the finite-temperature behavior close to the SRT. One example is the presence of canted states close to the SRT line. Compared with previous MC results for $\delta = 4.5$ [24], the phase diagram canted region becomes wider for $\delta = 6$, consistent with the zero-temperature phase diagram [16]. However, the range of values of η where the ground-state canted angle is different from 0 becomes extremely narrow as δ is increased further. Hence, our mean-field results suggest that those states would be present at finite temperature only very close to the SRT line for any realistic value of δ. Another example is the stripe width variation and the magnetization stripe profile change with η, which closely follow the zero-temperature behavior [16]. Moreover, the qualitative agreement between our MC simulations on wedges and experimental results on Fe/Ni ultrathin films [2] supports an inverse relationship between out-of-plane anisotropy and film thickness $\eta \sim 1/d$.

The correlation between the stripe width variation with the temperature and that with the anisotropy observed close to the SRT in the present simulations is another interesting fact. As previously pointed out [1], varying the film thickness (always in the ultrathin limit) produces an effect similar to that of changing the temperature, thus leading to an "inverse effective temperature" interpretation of the thickness. Considering the relation $\eta \sim 1/d$, this appears to be consistent with the similarity observed between the change in the magnetization profile when η is varied and that observed in Fe films when the temperature is varied [7]. This set of similarities suggests that a deeper analysis of the interplay between temperature and anisotropy could shed additional light on the origin of the strong stripe width variation with temperature observed in ultrathin magnetic films.

[1] O. Portmann, A. Vaterlaus, and D. Pescia, Nature **422**, 701 (2003).

[2] Y. Z. Wu, C. Won, A. Scholl, A. Doran, H. W. Zhao, X. F. Jin, and Z. Q. Qiu, Phys. Rev. Lett. **93**, 117205 (2004).

[3] C. Won, Y. Wu, J. Choi, W. Kim, A. Scholl, A. Doran, T. Owens, J. Wu, X. Jin, H. Zhao, and Z. Q. Qiu, Phys. Rev. B **71**, 224429 (2005).

[4] O. Portmann, A. Vaterlaus, and D. Pescia, Phys. Rev. Lett. **96**, 047212 (2006).

[5] O. Portmann, *Micromagnetism in the Ultrathin Limit* (Logos Verlag, Berlin, 2006).

[6] J. Choi, J. Wu, C. Won, Y. Z. Wu, A. Scholl, A. Doran, T. Owens, and Z. Q. Qiu, Phys. Rev. Lett. **98**, 207205 (2007).

[7] A. Vindigni, N. Saratz, O. Portmann, D. Pescia, and P. Politi, Phys. Rev. B **77**, 092414 (2008).

[8] N. Saratz, A. Lichtenberger, O. Portmann, U. Ramsperger, A. Vindigni, and D. Pescia, Phys. Rev. Lett. **104**, 077203 (2010).

[9] N. Saratz, U. Ramsperger, A. Vindigni, and D. Pescia, Phys. Rev. B **82**, 184416 (2010).

[10] N. Abu-Libdeh and D. Venus, Phys. Rev. B **81**, 195416 (2010).

[11] S. A. Cannas, D. A. Stariolo, and F. A. Tamarit, Phys. Rev. B **69**, 092409 (2004).

[12] R. Mulet and D. A. Stariolo, Phys. Rev. B **75**, 064108 (2007).

[13] S. A. Pighin and S. A. Cannas, Phys. Rev. B **75**, 224433 (2007).

[14] D. G. Barci and D. A. Stariolo, Phys. Rev. Lett. **98**, 200604 (2007).

[15] O. Portmann, A. Gölzer, N. Saratz, O. V. Billoni, D. Pescia, and A. Vindigni, Phys. Rev. B **82**, 184409 (2010).

[16] S. A. Pighín, O. V. Billoni, D. A. Stariolo, and S. A. Cannas, J. Magn. Magn. Mater. **322**, 3889 (2010).

[17] S. A. Cannas, M. Carubelli, O. V. Billoni, and D. A. Stariolo, Phys. Rev. B **84**, 014404 (2011).

[18] E. A. Jagla, Phys. Rev. E **70**, 046204 (2004).

[19] S. A. Cannas, M. F. Michelon, D. A. Stariolo, and F. A. Tamarit, Phys. Rev. B **73**, 184425 (2006).

[20] E. Rastelli, S. Regina, and A. Tassi, Phys. Rev. B **73**, 144418 (2006).

[21] L. Nicolao and D. A. Stariolo, Phys. Rev. B **76**, 054453 (2007).

[22] S. A. Cannas, M. F. Michelon, D. A. Stariolo, and F. A. Tamarit, Phys. Rev. E **78**, 051602 (2008).

[23] M. Carubelli, O. V. Billoni, S. A. Pighin, S. A. Cannas, D. A. Stariolo, and F. A. Tamarit, Phys. Rev. B **77**, 134417 (2008).

[24] J. P. Whitehead, A. B. MacIsaac, and K. De'Bell, Phys. Rev. B **77**, 174415 (2008).

[25] R. Diaz-Mendez and R. Mulet, Phys. Rev. B **81**, 184420 (2010).

[26] P. Politi, Comments Condens. Matter Phys. **18**, 191 (1998).

[27] Y. Yafet and E. M. Gyorgy, Phys. Rev. B **38**, 9145 (1988).

[28] D. Pescia and V. L. Pokrovsky, Phys. Rev. Lett. **65**, 2599 (1990).

[29] A. Vaterlaus, C. Stamm, U. Maier, M. G. Pini, P. Politi, and D. Pescia, Phys. Rev. Lett. **84**, 2247 (2000).

[30] A. B. Kashuba and V. L. Pokrovsky, Phys. Rev. B **48**, 10335 (1993).

[31] N. Goldenfeld, *Lectures on Phase Transitions and the Renormalization Group, Vol. 85. Frontiers in Physics* (Westview Press, Boulder, CO, 1992).

[32] P. Politi, A. Rettori, and M. G. Pini, Phys. Rev. Lett. **70**, 1183 (1993).